

Dynamics of three-dimensional helical domain wall in cylindrical NiFe nanowires

D. W. Wong, M. Chandra Sekhar, W. L. Gan, I. Purnama, and W. S. Lew

Citation: *Journal of Applied Physics* **117**, 17A747 (2015); doi: 10.1063/1.4919045

View online: <http://dx.doi.org/10.1063/1.4919045>

View Table of Contents: <http://scitation.aip.org/content/aip/journal/jap/117/17?ver=pdfcov>

Published by the [AIP Publishing](#)

Articles you may be interested in

[Micro-focused Brillouin light scattering study of the magnetization dynamics driven by Spin Hall effect in a transversely magnetized NiFe nanowire](#)

J. Appl. Phys. **117**, 17D504 (2015); 10.1063/1.4907612

[Control of domain wall pinning by localised focused Ga⁺ ion irradiation on Au capped NiFe nanowires](#)

J. Appl. Phys. **116**, 163901 (2014); 10.1063/1.4900437

[Depinning assisted by domain wall deformation in cylindrical NiFe nanowires](#)

J. Appl. Phys. **115**, 083913 (2014); 10.1063/1.4867004

[Helical domain walls in constricted cylindrical NiFe nanowires](#)

Appl. Phys. Lett. **101**, 152406 (2012); 10.1063/1.4758469

[Exchange biasing of a Néel wall in the nanocontact between NiFe wires](#)

J. Appl. Phys. **97**, 014309 (2005); 10.1063/1.1829143



You don't still use this cell phone



or this computer



Why are you still using an AFM designed in the 80's?



It is time to upgrade your AFM

Minimum \$20,000 trade-in discount for purchases before August 31st

Asylum Research is today's technology leader in AFM

dropmyoldAFM@oxinst.com



OXFORD INSTRUMENTS
The Business of Science®

Dynamics of three-dimensional helical domain wall in cylindrical NiFe nanowires

D. W. Wong, M. Chandra Sekhar, W. L. Gan, I. Purnama, and W. S. Lew^{a)}

School of Physical and Mathematical Sciences, Nanyang Technological University, 21 Nanyang Link, Singapore 637371

(Presented 4 November 2014; received 11 September 2014; accepted 4 January 2015; published online 24 April 2015)

We report on a micromagnetic study on the dynamics of current-driven helical domain wall (DW) in cylindrical NiFe nanowires. The helical DW is a three-dimensional transition region between magnetizations with clockwise and anticlockwise vortex orientations. A minimum current density is needed to overcome an intrinsic pinning to drive the helical DW, and the propagation along the nanowire is accompanied by a rotational motion. As the driving current strength is increased, the rotation ceases while the DW propagates at an increased velocity. However, a velocity barrier is experienced which results in the decrease of the DW mobility. Throughout its motion, the propagated helical DW maintains a stable profile without showing any sign of structural breakdown even at relatively high driving current. © 2015 AIP Publishing LLC. [<http://dx.doi.org/10.1063/1.4919045>]

Magnetic domain wall (DW) propagation in planar nanowires has been intensively studied both experimentally^{1–5} and theoretically^{6–8} with a focus to realize DW-based memory devices. One of the major technological limitations that are faced when using the planar nanowires is the occurrence of the Walker breakdown phenomenon, where the DW profile starts to break down under the application of high current or field.^{7,8} Therefore, the maximum velocity at which a DW can propagate in planar nanowires without changing the DW profile is restricted by the Walker limit. In cylindrical nanowires, it has been predicted that Walker breakdown is absent due to the geometrical symmetry of the cylindrical nanowires. Consequently, the DW profile in the cylindrical nanowire remains stable as it is allowed to rotate within the nanowire.^{9,10} Moreover, different types of DWs can be obtained depending on the diameters of the cylindrical nanowires. At a diameter of 350 nm, a three-dimensional helical DW is expected to form,^{11,12} while at diameters between 40 and 50 nm, a Bloch-point DW or a transverse DW is observed.^{13–15} Although the DW dynamics in planar nanowires are relatively well understood,^{16–18} there is very limited research work reported on the dynamics of the three-dimensional helical DWs.

In this work, the dynamics of current-driven helical DWs in cylindrical NiFe nanowires are investigated. Our simulation findings show that a minimum current density is needed to overcome the intrinsic pinning to drive the helical DW, in contrast to the transverse DW.¹⁰ The helical DW motion can be categorized into two distinct regions: low and high current density regimes. At low current density, the helical domain wall undergoes a rotation during its propagation, while at high current density, this rotation ceases. We also show that there is no limit on the maximum velocity of the helical DW due to the suppression of Walker breakdown.

However, a velocity barrier is experienced which results in a decrease in the DW mobility. In addition, we have investigated the current-driven depinning mechanisms of the helical DW in modulated nanowire which shows a greater dependence on the modulation depth rather than on the modulation length.

The dynamics of helical DW in the 350-nm-diameter cylindrical nanowire are studied by means of the Object Oriented Micromagnetic Framework (OOMMF),¹⁹ with the addition of the spin transfer torque (STT) term to the Landau–Lifshitz–Gilbert equation.²⁰ The material parameters used in the simulations correspond to permalloy (Ni₈₀Fe₂₀). The saturation magnetization (M_s) = 860×10^3 A/m, exchange stiffness constant (A_{ex}) = 1.3×10^{-11} J/m, and magnetocrystalline anisotropy (k) = 0. The Gilbert damping constant (α) and the non-adiabatic constant (β) are fixed at 0.005 and 0.04, respectively.^{21–26} Recent measurements indicate the β to be between 0.08 and 0.15,^{23–25} and the helical domain wall dynamics do not show any significant difference for all β values considered. A 350-nm-diameter cylindrical nanowire with a length of $2 \mu\text{m}$ was used and a unit cell size of $10 \text{ nm} \times 5 \text{ nm} \times 5 \text{ nm}$ was chosen for all simulations.¹¹ Selected simulations with smaller cell size of $5 \text{ nm} \times 5 \text{ nm} \times 5 \text{ nm}$ were also performed to observe the effect of the cell size on the simulation; similar results were obtained but with prolonged simulation time. Additional simulations were also performed on a micromagnetic simulation program with thermal fluctuations, Mumax³ (Ref. 27), to confirm the stability and dynamics of the helical DW at different temperatures (between 0 K and 300 K). Simulations that do not involve thermal function produced by both Mumax³ and OOMMF show consistent results.

Fig. 1(a) shows the simulated magnetization configuration of the 350-nm-diameter cylindrical nanowire. At relaxation state, a three-dimensional vortex magnetization with anticlockwise and clockwise orientations is formed at the opposite ends of the nanowire, as shown in the cross sectional

^{a)}Author to whom correspondence should be addressed. Electronic mail: wensiang@ntu.edu.sg.

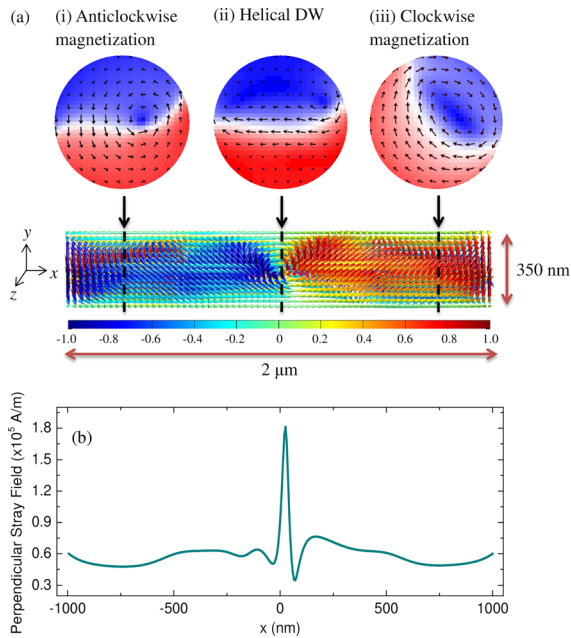


FIG. 1. (a) The magnetization configurations of a cylindrical NiFe nanowire with a diameter of 350 nm. Cross sectional view of the three-dimensional magnetization configurations showing anticlockwise (i) and clockwise (iii) vortex orientations at the ends of the nanowire, and the two vortices are connected *via* a gradual rotation of magnetization at the nanowire center, thus forming the helical DW (ii). (b) The extracted perpendicular stray field component of the nanowire is plotted against the x -axis of the nanowire, indicating a strong stray field in the perpendicular direction from the helical DW.

view in Figs. 1(a-i) and 1(a-iii), respectively. The two vortices gradually extend towards the center of the cylindrical nanowire and are eventually connected via the helical DW,^{11,12} as shown in Fig. 1(a-ii). The helical DW is in a stable state at the dimension of 350 nm.^{11,12} From the discretized magnetization $\mathbf{M}(\mathbf{r}_j)$ of the cylindrical nanowire, the demagnetization field $\mathbf{H}(\mathbf{r}_i)$ is expressed as

$$\mathbf{H}(\mathbf{r}_i) = - \sum_j \tilde{\mathbf{N}}(\mathbf{r}_i - \mathbf{r}_j) \mathbf{M}(\mathbf{r}_j), \quad (1)$$

where \mathbf{N} is the demagnetization tensor at each point in the nanowire.^{19,28} The stray field $\mathbf{H}(\mathbf{r}_i)$ created by the helical DW can then be calculated by applying the convolution theorem to Eq. (1)

$$\mathbf{H}(\mathbf{r}_i) = -\mathcal{F}^{-1}[\mathcal{F}(\tilde{\mathbf{N}}) \cdot \mathcal{F}(\mathbf{M})]. \quad (2)$$

Fig. 1(b) shows the calculated stray field profile of the nanowire along a line parallel to the x axis and at a distance of 10 nm from the nanowire surface. At the helical DW, the calculated peak stray field is approximately 1.8×10^5 A/m.

When a spin-polarized current is applied, the helical DW moves in the direction of the conduction electron flow due to the localized momentum transfer from the STT.²⁹ Fig. 2(a) shows the average helical DW velocity as a function of current density, which is determined by analyzing the time taken by the helical DW to travel from $x=0$ nm to $x=800$ nm. A minimum current density (J_i) for the helical DW to overcome its intrinsic pinning is found to be

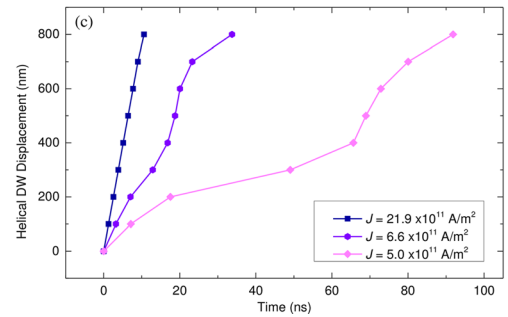
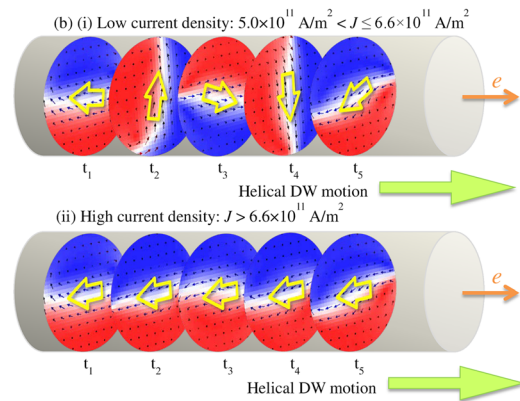
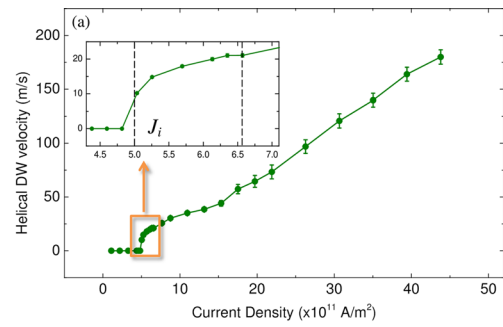


FIG. 2. (a) The average velocity of the helical DW with respect to the applied current density. Inset shows the close up data of the helical DW velocity for the range of applied current density $4.3\text{--}7.1 \times 10^{11}$ A/m². (b) A schematic illustration of the current driven helical DW motion. The cross sections indicate the orientation of the helical DW at successive moments in time. The yellow arrow illustrates the orientation of the helical DW (i) with a rotational motion at low current density (5.0×10^{11} A/m² $< J \leq 6.6 \times 10^{11}$ A/m²) and (ii) without a rotation at high current density ($J > 6.6 \times 10^{11}$ A/m²). (c) The displacement of the helical DW with respect to time, for $J = 5.0 \times 10^{11}$ A/m², 6.6×10^{11} A/m², and 21.9×10^{11} A/m² indicating the linear and non-linear motion of the helical DW.

5.0×10^{11} A/m², whereby the helical DW remains static with a current density that is lower than J_i . The helical DW motion can be categorized into two distinct regions: low and high current density regimes. When a low current density is applied, i.e., $5.0\text{--}6.6 \times 10^{11}$ A/m², a sharp slope of the helical DW velocity curve was observed, which is similar to the pre-breakdown regime in Walker's model.³⁰ At high current densities, i.e., $>6.6 \times 10^{11}$ A/m², the helical DW velocity increases near linearly thereafter without any discernable limit.

Figs. 2(b-i) and 2(b-ii) show the cross sections of the helical DW at successive moments in time with low and high current densities, respectively. At low current densities, the helical DW is observed to rotate about the nanowire axis as

it propagates in the nanowire. At high current densities, this rotation is found to be non-existent while the helical DW profile remains stable. This behavior is further illustrated in the DW displacement as a function of time, which shows that the instantaneous velocity of the helical DW becomes more uniform as the current density is increased, as shown in Fig. 2(c). The non-uniform helical DW velocity at low current density can be attributed to the loss in the energy due to its rotation, which deters the helical DW from Walker breakdown.⁹ At high current densities, the helical DW moves linearly with an increasing velocity due to the disappearance of the helical DW rotation. However, there is a sudden drop in the slope of the helical DW velocity curve, i.e., decrease in DW mobility owing to the suppressed Walker breakdown.³⁰ The helical DW profile is also observed to be stable even up to $5.0 \times 10^{12} \text{ A/m}^2$.

Multiple helical DWs can be formed in a single 350-nm-diameter cylindrical nanowire during the relaxation process by introducing modulations along the nanowire. The modulations function to separate the magnetization configuration of the nanowire into different regions. With the modulation length $l \leq 100 \text{ nm}$, the magnetization configuration of the diameter-modulated nanowire is similar to that of an unmodulated nanowire, where the anticlockwise and clockwise orientations are connected via a single helical DW, as shown in Fig. 1(a). However, when l is increased to 200 nm, an additional helical DW can be formed on the left and right sides of the modulation, as shown in Fig. 3(a). The simulation results revealed that a minimum $l > 100 \text{ nm}$ is required to allow the modulation to behave as a separator for the magnetization within the nanowire. For every n modulations with $l > 100 \text{ nm}$, there will be $2n + 1$ helical DWs formed in the cylindrical nanowire. The number of helical DWs formed is then found to be dependent on the modulation length and proportional to the number of modulations. Thus, it is possible to control the number of helical DWs that are present in the nanowire by varying the dimensions and number of modulations.

To investigate the depinning mechanism of the helical DW in a modulated cylindrical nanowire, spin-polarized current is applied to drive the helical DW across the modulations with different dimensions. First, d was kept constant at 250 nm while l was varied from 0 nm to 400 nm. The current density within the modulation is adjusted accordingly to the diameter of the modulation. The modulation is constructed cylindrically symmetric, concentric, and at the center with respect to the nanowire. A single helical DW was initially relaxed on the left, which is then driven across the modulation to the right of the nanowire. As shown in Fig. 3(b), the depinning current density increases sharply when the modulation is introduced and becomes relatively constant at the threshold depinning current density ($J_l \approx 10.1 \times 10^{11} \text{ A/m}^2$) for $l > 200 \text{ nm}$. For the helical DW to pass through the modulation, first it has to shrink to fit into the modulation and then expand back as it leaves the modulation. However, at $l < 200 \text{ nm}$, the pinning potential from the left and the right side of the modulation overlaps with each other, resulting in a larger overall pinning strength of the modulation.

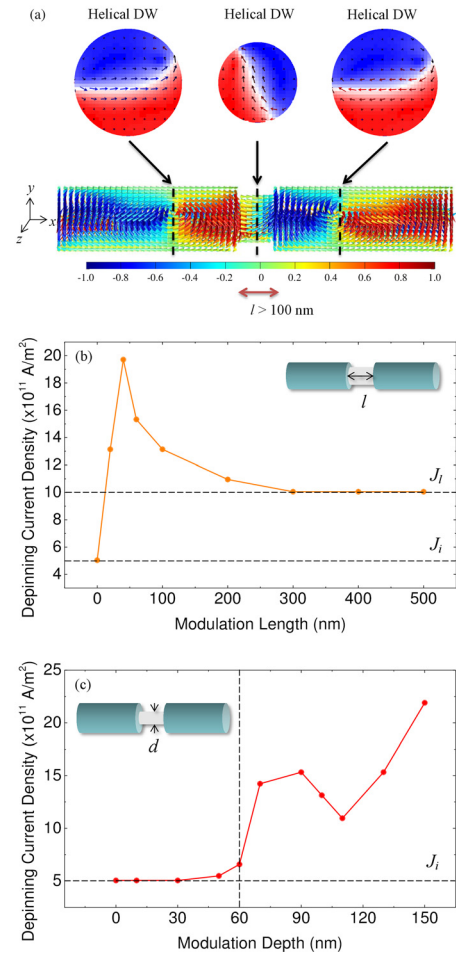


FIG. 3. (a) The magnetization configuration of a diameter-modulated cylindrical NiFe nanowire. The modulation has a length (l) of 200 nm and a diameter of 250 nm at the center. The nanowire is shown to possess three helical DWs on the left of the nanowire, in the modulation, and on the right of the nanowire. (b) Helical DW depinning current density as a function of the modulation length (l). The inset is the illustration of the modulated nanowire with a modulation length of l . (c) Helical DW depinning current density as a function of the modulation depth (d). The inset is the illustration of the modulated nanowire with a modulation depth of d .

Next, l was kept constant at 100 nm while the modulation diameter was varied between 240 nm and 350 nm. The depth of the modulation (d) is defined as the difference in diameter between the nanowire and the modulation. Similarly, a single helical DW was initially relaxed on the left, which is then driven across the modulation to the right of the nanowire. As shown in Fig. 3(c), the depinning current density increases with a deeper modulation. However, a minimum $d > 60 \text{ nm}$ is needed for the pinning of helical DW to be significant. With $d < 60 \text{ nm}$, the modulated cylindrical nanowire behaves like an unmodulated cylindrical nanowire, and the helical DW is able to move across the modulation without any significant pinning. At $d = 90 \text{ nm}$, the current density inside the modulation is approximately twice of that in the nanowire, which aids in decreasing the depinning current density of the helical DW. However, as $d > 110 \text{ nm}$, the pinning strength of the modulation starts to overwhelm the depinning force from the applied current, which results in a higher depinning current density. This shows that the pinning

strength of the modulation is largely dependent on d as compared to l . The phenomenon of the increase in the depinning current density at deeper modulation is also observed in planar nanowires,³¹ and hence the modulation acts as an adjustable pinning site for the helical DW.

In conclusion, our simulation findings predict some intriguing dynamics properties of a three-dimensional helical domain wall in 350-nm-diameter cylindrical NiFe nanowire when the motion is induced by the current-driven spin torque transfer effect. Unlike transverse DW, the helical DW has an intrinsic pinning to overcome before a motion can be initiated. The minimum current density for overcoming such pinning is estimated to be 5.0×10^{11} A/m². The velocity of the helical DW is found to be non-linear at lower current strength ($\leq 6.6 \times 10^{11}$ A/m²), and the propagation is also found to be accompanied by a rotational motion. At higher current strength, the DW propagates with a higher velocity but the rotational motion ceases. The profile of the helical DW remains stable at high current density with no sign of structural breakdown but with a decrease in DW mobility due to the suppression of Walker breakdown. In diameter-modulated nanowires, where multiple helical DWs can be stabilized, the DW pinning strength is found to be largely dependent on the modulation depth.

This work was supported by the Singapore National Research Foundation CRP grant (Non-Volatile Magnetic Logic and Memory Integrated Circuit Devices, NRF-CRP9-2011-01). We also wish to acknowledge the funding for this project from Nanyang Technological University under the

Undergraduate Research Experience on Campus (URECA) programme.

- ¹S. S. P. Parkin *et al.*, *Science* **320**, 190 (2008).
- ²M. Hayashi *et al.*, *Phys. Rev. Lett.* **98**, 037204 (2007).
- ³A. Yamaguchi *et al.*, *Phys. Rev. Lett.* **92**, 077205 (2004).
- ⁴M. Kläui *et al.*, *Appl. Phys. Lett.* **83**, 105 (2003).
- ⁵J. Grollier *et al.*, *Appl. Phys. Lett.* **83**, 509 (2003).
- ⁶L. D. Geng *et al.*, *J. Appl. Phys.* **112**, 083903 (2012).
- ⁷A. Mougin *et al.*, *Europhys. Lett.* **78**, 57007 (2007).
- ⁸A. Thiaville *et al.*, *Europhys. Lett.* **69**, 990 (2005).
- ⁹R. Wieser *et al.*, *Phys. Rev. B* **82**, 144430 (2010).
- ¹⁰M. Yan *et al.*, *Phys. Rev. Lett.* **104**, 057201 (2010).
- ¹¹M. Chandra Sekhar *et al.*, *Appl. Phys. Lett.* **101**, 152406 (2012).
- ¹²N. Biziere *et al.*, *Nano Lett.* **13**, 2053 (2013).
- ¹³R. Wieser *et al.*, *Phys. Rev. B* **69**, 064401 (2004).
- ¹⁴R. Hertel *et al.*, *Physica B* **343**, 206 (2004).
- ¹⁵H. G. Piao *et al.*, *Appl. Phys. Lett.* **102**, 112405 (2013).
- ¹⁶W. Zhu *et al.*, *Appl. Phys. Lett.* **101**, 082402 (2012).
- ¹⁷D. Atkinson *et al.*, *Appl. Phys. Lett.* **92**, 022510 (2008).
- ¹⁸M. Hayashi *et al.*, *Appl. Phys. Lett.* **92**, 162503 (2008).
- ¹⁹OOMMF Extension for Current-induced Domain Wall Motion developed by IBM Research, Zurich, see <http://www.zurich.ibm.com/st/magnetism/spintevolve.html> for the code implementing the two spin transfer torque terms (adiabatic and non-adiabatic) modifying the LLG equation.
- ²⁰M. J. Donahue and D. G. Porter, Interagency Report No. NISTIR 6376, National Institute of Standards and Technology, Gaithersburg, MD, 1999.
- ²¹L. Thomas *et al.*, *Nature* **443**, 197 (2006).
- ²²M. L. Schneider *et al.*, *Appl. Phys. Lett.* **87**, 072509 (2005).
- ²³M. Eltschka *et al.*, *Phys. Rev. Lett.* **105**, 056601 (2010).
- ²⁴L. Heyne *et al.*, *Phys. Rev. Lett.* **105**, 187203 (2010).
- ²⁵S. D. Pollard *et al.*, *Nat. Commun.* **3**, 1028 (2012).
- ²⁶M. Chandra Sekhar *et al.*, *J. Appl. Phys.* **115**, 083913 (2014).
- ²⁷A. Vansteenkiste *et al.*, *AIP Adv.* **4**, 107133 (2014).
- ²⁸C. Abert *et al.*, *IEEE Trans. Magn.* **48**, 1105 (2011).
- ²⁹G. S. D. Beach *et al.*, *J. Magn. Magn. Mater.* **320**, 1272 (2008).
- ³⁰M. Yan *et al.*, *Appl. Phys. Lett.* **99**, 122505 (2011).
- ³¹A. Himeno *et al.*, *Appl. Phys. Lett.* **87**, 243108 (2005).